Math. Model. Nat. Phenom.
Vol. 11, No. 5, 2016, pp. 103–118
DOI: 10.1051/mmnp/201611507

Stabilizing Role of Nonlocal Interaction on Spatio-temporal Pattern Formation

M. Banerjee[1] *, L. Zhang[2]
[1] Department of Mathematics & Statistics, IIT Kanpur, Kanpur, INDIA
[2] Department of Mathematics and Mathematical Statistics, Umea University, Umea, Sweden

Abstract. Here we study a spatio-temporal prey-predator model with ratio-dependent functional response and nonlocal interaction term in the prey growth. For a clear understanding of the effect of nonlocal interaction on the resulting stationary and non-stationary patterns, we consider the nonlocal interaction term in prey growth only to describe the nonlocal intra-specific competition due to limited resources for the prey. First we obtain the patterns exhibited by the basic model in the absence of nonlocal interaction and then explore the effect of nonlocal interaction on the resulting patterns. We demonstrate the stabilizing role of nonlocal interaction as it induces stationary pattern from periodic and chaotic regimes with an increase in the range of nonlocal interaction. The existence of multiple branches of stationary solutions, bifurcating from homogeneous steady-state as well as non-stationary patterns, is illustrated with the help of numerical continuation technique.

Keywords and phrases: Prey-predator, nonlocal interaction, Turing bifurcation, stationary pattern, global bifurcation.

Mathematics Subject Classification: 35B36, 37G15, 92C15

1. Introduction

Spatio-temporal pattern formation for interacting population models is an active area of research and is based upon the coupled nonhomogeneous parabolic type of partial differential equations

$$\frac{\partial u}{\partial t} = \frac{\partial^2 u}{\partial x^2} + f(u,\, v), \tag{1.1a}$$

$$\frac{\partial v}{\partial t} = d\frac{\partial^2 v}{\partial x^2} + g(u,\, v), \tag{1.1b}$$

subjected to non-negative initial conditions $u(x,0) \equiv u_0(x)$, $v(x,0) \equiv v_0(x)$ and appropriately chosen boundary conditions. Here population densities of two interacting species are denoted by $u(x,t)$ and $v(x,t)$ at time t and at the spatial point x. The two functions $f(u,v)$ and $g(u,v)$ describe the temporal interaction among the individuals of the two species at the particular location x and at time t. The effect of random movement of the individuals within their habitat is represented by the diffusion terms, and d is the ratio of the diffusion rates of the two populations. Here all the independent variables, dependent variables and

*Corresponding author. E-mail: malayb@iitk.ac.in

Published by EDP Sciences and available at http://www.mmnp-journal.org or http://dx.doi.org/10.1051/mmnp/201611507

the diffusion parameter d are dimensionless quantities and throughout this paper we consider the same formalism. The functions f and g also involve some dimensionless parameters representing various intra- and inter-specific interaction terms but are suppressed here for the sake of simplicity.

In this work we are interested in considering a prey-predator type interacting model and hence u and v are considered as the prey and predator population densities respectively. The intra- and inter-specific interactions among the prey and predator species, described by the functions $f(u(x,t), v(x,t))$ and $g(u(x,t), v(x,t))$, are considered to be the interaction between the individuals located at the spatial point x for the model (1.1). In case of spatio-temporal models for interacting population, it is assumed that the individuals can move from one location to another. Hence it is quite natural to assume that the individuals located at the spatial point x can have access to the resources located at point y. Similar assumption is also true for the inter-species interaction. Based upon this assumption we can extend the local model (1.1) to a more realistic model by incorporating suitable nonlocal interaction term(s).

Consider first a well known single species population model in order to describe a simple model with nonlocal interaction term. In terms of dimensionless variables, the spatio-temporal model of single species population growth with logistic growth law and local interaction is governed by the equation

$$\frac{\partial u}{\partial t} = d\frac{\partial^2 u}{\partial x^2} + u(1-u). \tag{1.2}$$

Note that d is representing the rate of diffusivity of u. Here $u^2(x,t)$ describes the intra-species competition term for the access to limited resources. In order to formulate the model with nonlocal interaction term, we assume that individuals located at point x can move to the point y to have access to the resources available at that point. Hence the individuals located at the point x will compete with the individuals of the same species located at y. As a result the nonlocal consumption of resources can be included into the model (1.2) by replacing the intra-species interaction term $u^2(x,t)$ by the expression

$$u(x,t)\int_{-\infty}^{\infty}\phi(x-y)u(y,t)dy,$$

where $\phi(x-y)$ is a kernel function representing the intensity of consumption/interaction and is also a function of the distance between the points x and y. Without any loss of generality we can assume that $\phi(\cdot)$ is an even function which in turn means that the movement is unbiased. Replacing the term $u^2(x,t)$ by the nonlocal term in (1.2), we get the desired model with nonlocal term as follows

$$\frac{\partial u}{\partial t} = d\frac{\partial^2 u}{\partial x^2} + u\left(1 - \int_{-\infty}^{\infty}\phi(x-y)u(y,t)dy\right). \tag{1.3}$$

This reaction-diffusion model with nonlocal interaction term represents the single species population growth with nonlocal intra-specific competition for limited resources in the context of ecology and is also capable to describe the emergence of biological species [8, 10, 23].

Analytical results and supportive numerical simulations of spatio-temporal models, with local interaction term, are capable to explain stationary and oscillatory/aperiodic patterns produced by the single species or multi-species interacting populations over their habitats. Analysis of the models of the form (1.1) or with two dimensional space can predict the stationary patches as well as time varying patches depending upon the magnitudes of model parameters. However, the spatio-temporal chaotic patterns are not well understood in the context of ecological interactions apart from the interaction between phytoplankton and zooplankton [12,13]. The phytoplankton bloom due to the interaction between phytoplankton and zooplankton can explain the spatio-temporal chaotic patterns obtained through numerical simulations. In case of other types of interacting population models, the spatio-temporal chaotic patterns are not well evident apart from a limited number of exceptions. Besides the parameter values, the generation of spatial patterns depends mostly on the reaction kinetics, *i.e.* the type of interaction among the interacting species. This mechanism is responsible for the absence of Turing pattern in the

Gause type prey-predator models where functional response is prey-dependent and intrinsic death rate of predator population is constant. However, such models can produce traveling wave, periodic traveling wave, spatio-temporal chaotic pattern which are labeled as non-Turing patterns [3, 4]. These non-Turing patterns describe a continuous change in the population patches and never converge to any stationary distribution.

Spatio-temporal prey-predator models with ratio dependent functional response and local interaction terms exhibit a wide variety of stationary and non-stationary patterns [2–4]. The non-stationary patterns are observed for the the parameter values mostly within the Turing-Hopf domain. The range of parameter values for which we can find stationary patterns is significantly less compared to the range of parameter values leading to non-stationary patterns when the ratio of diffusivities (*i.e.* d) is small. Recently we have proved the stabilizing role of nonlocal interaction term leading to stationary patterns over a large range of parameter values [5]. We have also established the existence of multiple stationary branches of solution implying the extension of stationary patch sizes as an evolutionary behavior. However the emergence of stationary patchy patterns from periodic and/or aperiodic patterns remains an open question.

The main objective of the present work is to answer the above question by working on a spatio-temporal model, with ratio-dependent functional response, where nonlocal consumption of resources is considered in the context of intra-species competition for prey species. Nonlocal interaction term is introduced into the growth equation of prey population only. In section 2 the main features of the temporal model and spatio-temporal model with local interaction are described briefly. Formulation of the spatio-temporal model with nonlocal interaction is described in section 3 along with the linear stability results and the conditions for Turing and spatial Hopf bifurcations. Extensive numerical simulation results to validate the analytical findings and to identify the relevant bifurcations are given in section 4. The results of this work are summarized in section 5 along with a brief discussion for possible future developments of this work.

2. Basic model

The present work is based upon a Michaelis-Menten type prey-predator model with ratio-dependent functional response and density dependent death rate of predator [2]. In terms of the dimensionless variables and parameters, the basic temporal model is governed by the following system of nonlinear coupled ordinary differential equations

$$\frac{du}{dt} = u(1-u) - \frac{\alpha uv}{u+v} \equiv f(u,v), \tag{2.1a}$$

$$\frac{dv}{dt} = \frac{\beta uv}{u+v} - \gamma v - \delta v^2 \equiv g(u,v), \tag{2.1b}$$

subjected to non-negative initial conditions $u(0), v(0) \geq 0$. Here $u \equiv u(t)$, $v \equiv v(t)$ denote the population densities of prey and predator respectively at any time t assuming their homogeneous distribution over space. α, β, γ and δ are all positive dimensionless parameters and represent the grazing rate of prey by predators, prey-dependent growth rate of predators, death rate of predators and strength of intra-specific competition among the predators respectively. All of them are re-scaled parameters. The model (2.1) exhibits a wide variety of local and global bifurcations depending upon the parametric restrictions [2]. Here we just mention the parametric conditions required for the feasible existence of interior equilibrium point and the conditions for Hopf-bifurcation without going into the details. These results are required for the subsequent discussions.

The temporal model (2.1) admits at most two interior equilibrium points. If we denote them by $E_{j*}(u_{j*}, v_{j*})$, the associated components are given by

$$u_{j*} = \frac{\alpha(\gamma - 2\beta + \delta) + 2\beta + (-1)^j \sqrt{\alpha^2(\gamma-\delta)^2 + 4\alpha^2\beta\delta + 4\alpha^3\delta(\gamma-\beta)}}{2(\beta + \alpha\delta)}$$
$$v_{j*} = \frac{u_{j*}(1-u_{j*})}{u_{j*} + \alpha - 1},\ j = 1, 2.$$

There exist two different sets of parametric restrictions under which the model (2.1) has a unique interior equilibrium point. Such parametric restrictions are given by, **H1**: $0 < \alpha < 1$ and $\beta > \gamma$; **H2**: $\alpha > 1$ and $0 < \gamma < \beta < \frac{1}{\alpha} + \frac{\gamma}{\delta} - 1$. The unique equilibrium point is E_{2*}. We find two interior equilibria under the parametric restriction **H3**: $\alpha > 1$ and $0 < \max\left\{\gamma, \frac{\alpha\gamma}{\alpha-1}, \frac{1}{\alpha} + \frac{\gamma}{\delta} - 1\right\} < \beta < \frac{(\gamma-\delta)^2 + 4\alpha\gamma\delta}{4\delta(\alpha-1)}$, (see [2] for details).

The local asymptotic stability of the interior equilibrium points is determined by the sign of eigenvalues of the Jacobian matrix for the system (2.1) and evaluated at the concerned equilibrium point. If E_* denotes a typical interior equilibrium point, the stability conditions are given by

$$a_{11} + a_{22} < 0, \tag{2.2a}$$
$$a_{11}a_{22} - a_{12}a_{21} > 0, \tag{2.2b}$$

where

$$a_{11} = f_u(u_*, v_*),\ a_{12} = f_v(u_*, v_*),\ a_{21} = g_u(u_*, v_*),\ a_{22} = g_v(u_*, v_*).$$

In terms of the parameter α, the Hopf-bifurcation condition is given by

$$a_{11} + a_{22}\big|_{\alpha=\alpha_H} = 0, \tag{2.3a}$$
$$a_{11}a_{22} - a_{12}a_{21}\big|_{\alpha=\alpha_H} > 0, \tag{2.3b}$$
$$\left[\frac{d}{d\alpha}a_{11}\right]_{\alpha=\alpha_H} \neq 0, \tag{2.3c}$$

where α_H is the Hopf-bifurcation threshold. The Hopf-bifurcating limit cycle may be stable or unstable and is determined by the first Lyapunov number [11,19]. For the model (2.1), we find a stable equilibrium surrounded by an unstable limit cycle as well as the unstable equilibrium enclosed by a stable limit cycle [2].

The spatio-temporal model corresponding to the temporal model (2.1), by incorporating self-diffusion terms, is given by

$$\frac{\partial u}{\partial t} = u(1-u) - \frac{\alpha uv}{u+v} + \frac{\partial^2 u}{\partial x^2}, \tag{2.4a}$$
$$\frac{\partial v}{\partial t} = \frac{\beta uv}{u+v} - \gamma v - \delta v^2 + d\frac{\partial^2 v}{\partial x^2}, \tag{2.4b}$$

for $x \in [-L, L] \subset \mathbb{R}$ and d is the ratio of diffusivity of the two species. The model (2.4) is subjected to non-negative initial conditions and periodic boundary conditions.

The components of the interior equilibrium points E_{j*} correspond to homogeneous steady-state for the system (2.4). Instability of a homogeneous steady-state, due to small amplitude heterogeneous perturbation around it, is known as the Turing instability. Here the Turing instability can occur around E_{2*} only. Other interior equilibrium point, when exists, is a saddle-point and fails to satisfy one of the conditions

for Turing instability as mentioned below. The Turing instability conditions are given by [16, 18]

$$a_{11} + a_{22} < 0, \tag{2.5a}$$

$$a_{11}a_{22} - a_{12}a_{21} > 0, \tag{2.5b}$$

$$da_{11} + a_{22} > 2\sqrt{d(a_{11}a_{22} - a_{12}a_{21})}, \tag{2.5c}$$

and the equation of the Turing bifurcation curve is

$$da_{11} + a_{22} = 2\sqrt{d(a_{11}a_{22} - a_{12}a_{21})}. \tag{2.6}$$

We have considered various types of spatio-temporal pattern formation by the model (2.4) with two dimensional space and no-flux boundary conditions and obtained various types of stationary and non-stationary patterns [2]. Here we present the bifurcation of stationary pattern from homogeneous steady-state and the transition to non-stationary patterns. Here we use forward and backward continuation method to determine the transition of spatial patterns. We fix the parameter values $\beta = 1$, $\gamma = 0.6$, $\delta = 0.1$. One can verify that the model (2.1) has only one interior equilibrium point for $\alpha < 1$ and it is globally asymptotically stable. For $\alpha > 1$, the equilibrium point E_{2*} is stable up to $\alpha < 2.008701006 \equiv \alpha_H$ and then loses stability through super-critical Hopf-bifurcation at $\alpha = 2.008701006$.

3. Nonlocal model

Here we first describe the nonlocal spatio-temporal model of prey-predator interaction governed by the following two coupled integro-differential equations

$$\frac{\partial u(t,x)}{\partial t} = u(t,x)(1 - w(t,x)) - \frac{\alpha u(t,x)v(t,x)}{u(t,x) + v(t,x)} + \frac{\partial^2 u(t,x)}{\partial x^2}, \tag{3.1}$$

$$\frac{\partial v(t,x)}{\partial t} = \frac{\beta u(t,x)v(t,x)}{u(t,x) + v(t,x)} - (\gamma + \delta v(t,x))v(t,x) + d\frac{\partial^2 v(t,x)}{\partial x^2}, \tag{3.2}$$

where

$$w(t,x) = \int_{-\infty}^{\infty} \phi(x-y)u(t,y)dy.$$

The nonlocal model is subjected to the positive initial condition and periodic boundary condition over $[-L, L]$. In this paper we consider the kernel function given by

$$\phi(z) = \begin{cases} \frac{1}{2M}, & |z| \le M \\ 0, & |z| > M \end{cases}. \tag{3.3}$$

The kernel function is an even function and this choice ensures that the homogeneous steady-states of the local model (2.4) is also the homogeneous steady-state for the nonlocal model (3.1). The intra-specific competition between the prey individuals is limited among the individuals located at a particular location 'x' only for the model (2.4). The model with nonlocal interaction term assumes that the intra-specific competition between the prey individuals is not limited to the individuals located at the point x only at any time. Any prey individual located at x can compete with other prey individuals located at some other point y for resource. Accordingly the intra-species competition rate for prey is determined by the integral $\int_{-\infty}^{\infty} \phi(x-y)u(t,y)dy$. The kernel function ϕ is the measure of the efficiency of competition for prey located at x with the prey located at the point y. The strength, or efficiency, of the nonlocal competition is proportional to the distance between the points x and y although it is assumed to be constant. Hence we can assume that the efficiency of intra-specific competition among the prey individuals depends on the distance between the locations of concerned individuals, as the interaction is zero outside the interval $[x - M, x + M]$ centered at the point x. Hence the negative feedback on the prey growth rate due to the nonlocal consumption of resources and hence the modified intra-specific competition is described by the

expression $u(t,x)\int_{-\infty}^{\infty}\phi(x-y)u(t,y)dy$ and by $u(t,x)\int_{-M}^{M}\frac{u(t,y)}{2M}dy$ for the specific kernel function ϕ as defined in (3.3).

In [22], the authors have considered some asymmetric kernel functions and studied the resulting pattern formation. However, the assumption that the kernel function ϕ is an even function has some merit as it represents the unbiased movement of the individuals around their average location. Also the consideration of ϕ as an even function makes it easy to derive the analytical results. The reaction-diffusion model itself assumes that the unbiased random movement over a slower time scale and it is quite reasonable to assume unbiased movement of the individuals related with nonlocal interactions. In [17], the authors have provided some estimates for the suitable kernel functions based upon field data and all of them are even functions.

3.1. Turing and spatial Hopf bifurcation

In Section 2, we have mentioned that the Turing instability can set in around the homogeneous coexisting steady-state E_{2*} only. The kernel function ϕ defined above, satisfies the condition $\int_{-\infty}^{\infty}\phi(z)dz = 1$ and hence $u(t,x) = u_{2*}$, $v(t,x) = v_{2*}$ is a homogeneous steady-state for the system (3.1) also. Here we derive the conditions for Turing and Turing-Hopf bifurcations around the homogeneous steady-state E_{2*} for the general form of kernel function $\phi(z)$. Linearizing the system (3.1) around the homogeneous steady state E_{2*} we find the following linear equations in terms of the perturbation variables u_1 and v_1

$$\lambda u_1(x) = (a_{11}+u_{2*})u_1(x) - u_{2*}\int_{-\infty}^{\infty}\phi(x-y)u_1(y)dy + a_{12}v_1(x) + u_1''(x), \tag{3.4a}$$

$$\lambda v_1(x) = a_{21}u_1(x) + a_{22}v_1(x) + dv_1''(x). \tag{3.4b}$$

Taking Fourier transform on both sides of these two equations, we get

$$\lambda\overline{u}_1(\xi) = (a_{11}+u_{2*})\overline{u}_1(\xi) - u_{2*}\overline{u}_1(\xi)\overline{\phi}(\xi) + a_{12}\overline{v}_1(\xi) - \xi^2\overline{u}_1(\xi), \tag{3.5a}$$

$$\lambda\overline{v}_1(\xi) = a_{21}\overline{u}_1(\xi) + a_{22}\overline{v}_1(\xi) - d\xi^2\overline{v}_1(\xi), \tag{3.5b}$$

where $\overline{u}_1(\xi)$, $\overline{v}_1(\xi)$ and $\overline{\phi}(\xi)$ denote the Fourier transforms of the functions $u_1(x)$, $v_1(x)$ and ϕ respectively. Stability of the homogeneous steady-state E_{2*} under small amplitude heterogeneous perturbations demands the satisfaction of following two inequalities

$$\Upsilon(\xi,M) \equiv a_{11}+a_{22}+u_{2*}-(1+d)\xi^2 - u_{2*}\overline{\phi}(\xi) < 0, \tag{3.6}$$

$$\Delta(\xi,M) \equiv \left[(a_{11}+u_{2*}) - u_{2*}\overline{\phi}(\xi) - \xi^2\right]\left[a_{22}-d\xi^2\right] - a_{12}a_{12} > 0. \tag{3.7}$$

With these definitions we can write the characteristic equation associated with the system (3.5) in the compact form

$$\lambda^2 - \Upsilon(\xi,M)\lambda + \Delta(\xi,M) = 0. \tag{3.8}$$

From above two expressions we find $\Upsilon(0,0) = a_{11}+a_{22}$ and $\Delta(0,0) = a_{11}a_{22}-a_{12}a_{21}$ where a_{ij}'s are defined earlier and evaluated at E_{2*}. Now we can define the conditions for Turing bifurcation and spatial Hopf-bifurcation precisely as follows

$$\Upsilon(0,0) < 0,\ \Delta(0,0) > 0,\ \Upsilon(\xi_T,M_T) < 0,\ \Delta(\xi_T,M_T) = 0, \tag{3.9}$$

and

$$\Upsilon(0,0) < 0,\ \Delta(0,0) > 0,\ \Upsilon(\xi_{SH},M_{SH}) = 0,\ \Delta(\xi_{SH},M_{SH}) > 0. \tag{3.10}$$

respectively. In the following subsection we derive the explicit Turing and spatial Hopf-bifurcation thresholds for the kernel function ϕ defined in (3.3).

3.2. Turing and spatial Hopf bifurcation conditions

To derive the Turing and spatial Hopf-bifurcation thresholds with the kernel function ϕ as defined at (3.3), we use $\overline{\phi}(\xi) = \frac{\sin \xi M}{\xi M}$. We find Turing instability condition by reversing the inequality (3.7). The condition for Turing instability is given by $\Delta(\xi, M) < 0$ where

$$\Delta(\xi, M) \equiv d\xi^4 - \left[da_{11} + a_{22} + du_{2*} - du_{2*}\frac{\sin(\xi M)}{\xi M}\right]\xi^2 + \left(a_{11} + u_{2*} - u_{2*}\frac{\sin(\xi M)}{\xi M}\right)a_{22} - a_{12}a_{21}. \quad (3.11)$$

To determine the stability boundary, we need to determine the thresholds for ξ and M such that only one eigenvalue of the characteristic equation (3.8) crosses the origin from left to right and other eigenvalues have negative real parts. The stability boundary in terms of ξ and M is determined by the solutions of the equations

$$\Delta(\xi, M) = 0, \ \frac{\partial \Delta(\xi, M)}{\partial \xi} = 0, \ \frac{\partial \Delta(\xi, M)}{\partial M} = 0. \quad (3.12)$$

Differentiating $\Delta(\xi, M)$ with respect to M and then equating to zero, we get

$$\left[du_{2*}\xi^2 - a_{22}\right]\left[\frac{\cos(\xi M)}{M} - \frac{\sin(\xi M)}{\xi M^2}\right] = 0,$$

and hence the required condition reduces to

$$\tan(\xi M) = \xi M. \quad (3.13)$$

Writing z for ξM in the above expression, we get $\tan z = z$. The positive roots of this equation are denoted by z_j satisfying $0 < z_1 < z_2 < ...$ and further we define $\mu_j = \frac{\sin z_j}{z_j}$. Using the condition $\frac{\partial \Delta(\xi, M)}{\partial \xi} = 0$ we get,

$$(da_{11} + du_{2*}(1 - \mu_j) + a_{22})^2 = 4d(a_{11}a_{22} + u_{2*}(1 - \mu_j)a_{22} - a_{12}a_{21}) \quad (3.14)$$

and then $\Delta(\xi, M) = 0$ gives

$$\xi_{Tj}^2 = \frac{(da_{11} + a_{22}) + du_{2*}(1 - \mu_j)}{2d}, \ j = 1, 2, 3, \cdots. \quad (3.15)$$

Using the relation $z = \xi M$, we find

$$M_{Tj} = \frac{z_j\sqrt{2d}}{\sqrt{(da_{11} + a_{22}) + du_{2*}(1 - \mu_j)}}, \ j = 1, 2, 3, \cdots. \quad (3.16)$$

The suffix T indicates the thresholds related to Turing instability and the admissible set of ξ_{Tj} and M_{Tj} depends on the chosen parameter values. These thresholds determine the alteration of the Turing domain for the model with nonlocal interaction when compared with its local counterpart. We explain this idea in the next section with appropriate numerical example.

Now we determine the spatial Hopf-bifurcation threshold. For this purpose we need to solve the equations

$$\Upsilon(\xi, M) = 0, \ \frac{\partial \Upsilon(\xi, M)}{\partial \xi} = 0, \ \frac{\partial \Upsilon(\xi, M)}{\partial M} = 0. \quad (3.17)$$

Proceeding in a similar fashion as above, we find the desired thresholds

$$\xi_{SHj}^2 = \frac{a_{11} + u_{2*}(1 - \mu_j) + a_{22}}{1 + d}, \ M_{SHj} = \frac{z_j\sqrt{1 + d}}{\sqrt{a_{11} + u_{2*}(1 - \mu_j) + a_{22}}}, \ j = 1, 2, 3, \cdots. \quad (3.18)$$

It is important to note that above thresholds will imply onset of oscillatory patterns through Hopf-bifurcation if in the vicinity of (ξ_{SHj}, M_{SHj}) the expression $\Delta(\xi, M)$ is positive. In the next section we will illustrate the analytical results with numerical example and obtain the resulting patterns with the help of extensive numerical simulations.

4. Numerical examples and pattern formation

In this section we present the spatio-temporal patterns produced by the basic spatio-temporal model (2.4) and then compare with the patterns produced by the nonlocal model (3.1) with the kernel function ϕ_1. We are mainly interested to detect the transition of spatial patterns from one type to another and how the nonlocal term influences the spatial pattern formation. The effect of the choice of kernel function to describe the nonlocal interaction is briefly described in the discussion section.

4.1. Pattern formation in local model

To explore the various types of pattern formation by the model (2.4), we fix the parameter values $\beta = 1$, $\gamma = 0.6$ and $\delta = 0.1$. We choose $d = 8$ and numerically simulate the model (2.4) for a range of parameter values $\alpha \in [1.9, 2.3]$. Turing instability condition is satisfied for $\alpha \geq 1.9$ for $d = 8$ and there is no feasible coexisting homogeneous steady-state for $\alpha > 2.32$ for chosen other parameter values. Hence we restrict ourselves within this range of α for the time being. We perform the numerical simulation over a spatial domain of size $[-400, 400]$ and the concerned model is subjected to the periodic boundary condition and we use the initial condition as follows,

$$u(0,x) = \begin{cases} u_{2*} + 0.1, & |x| \leq 1, \\ u_{2*}, & \text{elsewhere,} \end{cases} \qquad v(0,x) = \begin{cases} v_{2*} + 0.05, & |x| \leq 1, \\ v_{2*}, & \text{elsewhere,} \end{cases} . \tag{4.1}$$

Through numerical simulation we find stationary pattern for $\alpha \in [1.94, 2.17)$, oscillatory patterns for $\alpha \in (2.18, 2.2)$ and then spatio-temporal chaotic patterns for $\alpha \in (2.2, 2.25)$ and again we observe oscillatory pattern for $\alpha > 2.25$. This observation is in accordance with the patterns produced by the same model but with two dimensional space and no-flux boundary condition [2]. The oscillatory pattern can be distinguished from the stationary pattern by looking at the time evolution of spatial average for the prey and predator populations. The spatial average is taken over the entire space. Sometimes the initial transients persist over a longer time period. We have performed the numerical simulation over a sufficiently longer time in order to eliminate the initial transients and to determine the appropriate nature of the patterns. Three different types of patterns are presented at Fig. 1. The pattern presented at panel (b) seems to be similar with the pattern presented at panel (a) however a closer look (zoom view) can reveal that the boundary of vertical strips are not straight lines at panel (b). The time evolution of spatial average corresponding to the patterns presented at panels (b) and (c) exhibit regular and chaotic oscillations respectively, but we omit those figures here from the sake of brevity.

In order to understand the change in pattern formation with the increasing magnitude of α we have constructed a bifurcation diagram (see Fig. 2) with the plot of $\langle u \rangle$ against a range of values of α, keeping other parameters fixed. With the variation of α, we find three different types of patterns, stationary pattern (SP), oscillatory pattern (OP) and spatio-temporal chaotic pattern (STC) and the spatial distribution for these patterns is presented in the three panels of Fig. 1. The oscillatory patterns (spatial distribution is periodic in space as well as time) are obtained at two different parametric range and their qualitative features are the same, however the width of the patches are little bit different. For stationary pattern we have plotted $\langle u \rangle$ obtained from its stationary value. In case of oscillatory pattern and spatio-temporal chaos we never find a steady-state or stationary value of $\langle u \rangle$ and hence we have taken an average of $\langle u \rangle$ over a significantly longer time interval. The computation of $\langle u \rangle$ for stationary and dynamic patterns are explained in the appendix.

Now we use forward and backward continuation method to obtain another bifurcation diagram to understand the transition of patterns from one type to another (see Fig. 3). To prepare the bifurcation diagram first we have performed the numerical simulation for $\alpha = 2$ keeping other parameters fixed and the initial condition (4.1). The steady-state distribution obtained for $\alpha = 2$ is considered as the initial condition for simulation with $\alpha = 2.01$, other parameters remain unchanged. We collect the steady-state value of spatial average. Again the stationary distributions for u and v are used for the next simulation with $\alpha = 2.02$ and continued in forward direction until the stationary patterns persist. Similarly the

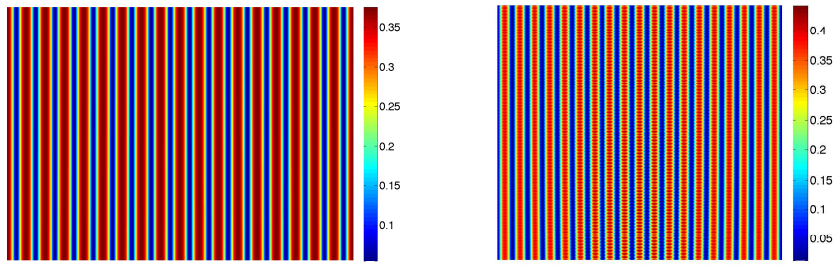

(a) (b)

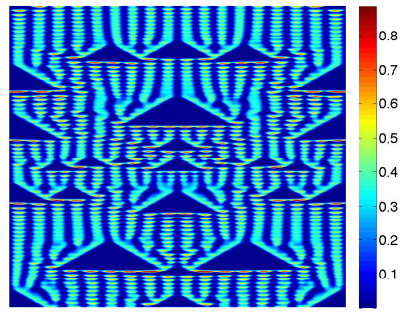

(c)

FIGURE 1. Numerical simulation result of the spatio-temporal model (2.4) for $\beta = 1$, $\gamma = 0.6$, $\delta = 0.1$, $d = 8$ and three different values of α. We find (a) stationary Turing pattern for $\alpha = 2.1$, (b) oscillatory pattern for $\alpha = 2.18$ and (c) spatio-temporal chaotic pattern for $\alpha = 2.25$. In each panel, the horizontal and vertical axes represent space and time respectively.

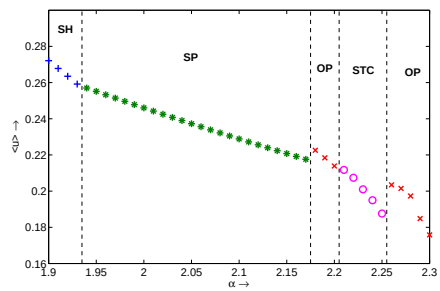

FIGURE 2. Bifurcation diagram against the parameter α, other parameters are fixed at $\beta = 1$, $\gamma = 0.6$, $\delta = 0.1$ and $d = 8$. For a range of values of α we find - stationary homogeneous (SH) distribution, stationary pattern (SP), oscillatory pattern (OP) and spatio-temporal chaotic (STC) pattern.

steady-state distribution obtained at $\alpha = 2$ is also used in the simulation for $\alpha = 1.99$ and this process is continued for lower values of α and we collect the spatial averages for each value of α. The branch of stationary pattern is presented in green colour. In the backward direction it converges to the homogeneous

steady-state and in forward direction it continues up to $\alpha = 2.19$ and then jumps to the extinction steady-state (this branch is not shown here). Next we simulate the model (3.1) with the initial condition (4.1) for $\alpha = 2.18$ and find oscillatory pattern. Again we perform the forward and backward continuation to determine the branch corresponding to the oscillatory pattern. For each value of α, we calculate $\langle u \rangle$ as described in the appendix and the obtained branch is presented in red colour. In the backward and forward direction, this branch terminates at the branches of stationary and chaotic patterns respectively. Adopting this forward and backward continuation method we determine a branch of spatio-temporal pattern and another branch of oscillatory patterns. Here we would like to mention that we have determined single branch with the help of forward and backward continuation method. However, there exist more than one branch of oscillatory and chaotic patterns for $\alpha > 2.2$. In this parametric range, the resulting patterns are highly sensitive to the initial conditions. The shape of the bifurcating branch will change depending on the value of α from which we are starting. For example, we have started our the numerical simulation from $\alpha = 2.26$ and the branch of oscillatory solution is obtained by forward as well as backward continuation. Instead, if we start from $\alpha = 2.27$ or 2.28 then we will get a different branch. It is important to mention here that the bifurcation thresholds are calculated correct up to two decimal place however their actual value may be little bit different but should be very close to the values we have obtained.

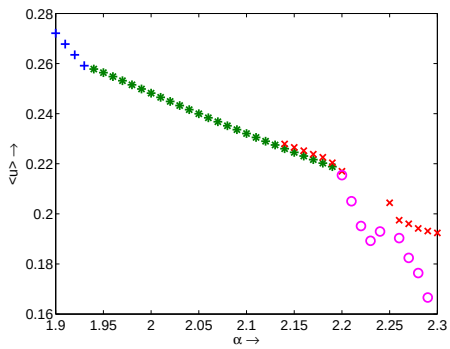

FIGURE 3. Bifurcation diagram obtained through forward and backward continuation.

The transition from homogeneous stationary state to stationary pattern then to oscillatory pattern and so on takes place at different thresholds of α with the variation of d. We need to keep in mind that the possibility of existence of more than one pattern for a particular set of parameter value mostly depends upon the choice of initial condition. This can be clearly understood if we compare the bifurcation diagrams presented at Fig. 2 and Fig. 3. Finally we want to present a complete pattern diagram for fixed values of $\beta = 1$, $\gamma = 0.6$, $\delta = 0.1$ and a range parameter values of α and d. The pattern diagram is presented at Fig. 4. For each choice of α, we have calculated the homogeneous steady-state and then performed numerical simulation with a range of values of d. For each choice of α and d we have identified the nature of resulting pattern and the outcomes are summarized in the pattern diagram. This pattern diagram reveals the possibility of extinction of both the species and also identifies the set of parameter values for which the homogeneous steady-state is stable. Obtained heterogeneous patterns are classified as stationary patterns, oscillatory patterns and spatio-temporal chaotic pattern. It is important to mention here that the transition of patterns observed for $d = 8$ at the pattern diagram (see Fig. 4) is not matching with the Fig. 2 as we have used forward continuation method to prepare the bifurcation diagram presented in Fig. 2.

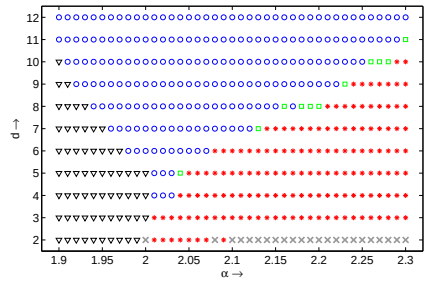

FIGURE 4. Pattern diagram for $\beta = 1$, $\gamma = 0.6$, $\delta = 0.1$ and a range of values of α and d. The symbol represents $\nabla \to$ homogeneous stationary state; o $\to$ stationary pattern; $\square \to$ oscillatory pattern; $* \to$ spatio-temporal chaos; x $\to$ extinction.

4.2. Pattern formation in nonlocal model

In this subsection we illustrate the Turing instability and spatial Hopf instability condition in details. First we explain the capability of nonlocal interaction leading to stationary patterns through Turing bifurcation with the parameter value(s) for which the local model fails to produce any spatial pattern. We choose the parameter values $\alpha = 1.9$, $\beta = 1$, $\gamma = 0.6$, $\delta = 0.1$ and $d = 2$. With this choice, we find $u_{2*} = 0.2721065248$ and $v_{2*} = 0.1689817092$ as the interior equilibrium point for (2.1) and homogeneous steady-state for (2.4) as well as (3.1). Interior equilibrium point (u_{2*}, v_{2*}) is locally asymptotically stable, with respect to the model (2.1). Small amplitude heterogeneous perturbation around the homogeneous steady-state for the local model (2.4) is unable to produce any stationary pattern, for the chosen parameter values, as the inequality (2.5c) is violated for chosen value of d. One can easily determine the Turing bifurcation threshold M_T by finding the value of M for which the curve (3.11) touches ξ-axis. Numerical computation reveals such threshold $M_T = 5.118$. The existence of this threshold, related with the sign of $\Delta(\xi, M)$, is illustrated in Fig. 5 for three different values of M. Now the natural question arises about the use of the Turing instability thresholds described at subsection 3.2. Due to the implicit nature of the equation (3.11), it is difficult to provide explicit expression for the Turing bifurcation thresholds analytically and hence we have described one way to determine the pair (ξ_{Tj}, M_{Tj}) to get any idea about the suitable choice of M to obtain stationary Turing pattern in the nonlocal model. Interestingly, the admissible values of M_{Tj} correspond to the patches of different widths depending on the choice of parameter values and the size of spatial domain.

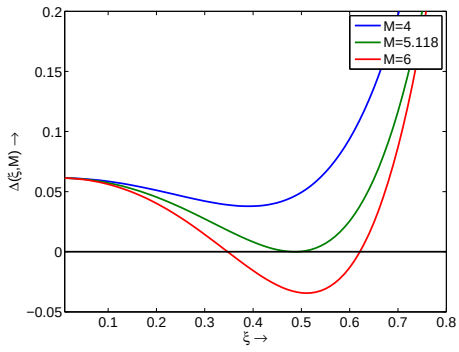

FIGURE 5. Plot of $\Delta(\xi, M)$ for three different values of M against ξ.

One can obtain the threshold pairs by using the positive roots of the equation $\tan z = z$. First three consecutive positive roots of the equation $\tan z = z$ are $z_1 = 4.49$, $z_2 = 7.73$ and $z_3 = 10.9$ approximately. The admissible values of z_j are determined by the positivity of the expression involved in (3.15) for chosen values of the parameters. Using the parameter values as mentioned above and the values of z_j, first we calculate $\mu_1 = -.2172323649$, $\mu_2 = 0.1283731070$ and $\mu_3 = -0.09132442691$ respectively. With these values of μ_j, from equations (3.15) and (3.16) we get the thresholds $M_{T1} = 10.28009175$, $M_{T2} = 20.38845204$ and $M_{T3} = 26.15821425$ respectively. The existence of more than one admissible values of M_{Tj} indicates the existence of multiple stationary branches. Now we illustrate the existence of multiple branches of stationary solutions with the help of numerical simulations.

The existence of multiple branches of stationary solution with the variation of M and the related simulation results are summarized at Fig. 6. First we have simulated the model (3.1) for $\alpha = 1.9$, $\beta = 1$, $\gamma = 0.6$, $\delta = 0.1$, $d = 2$ and $M = 10$, we find stationary pattern - the resulting pattern is stationary in time and oscillatory in space. The final distribution is used as the initial condition for next simulation with $M = 11$ and so on. For each value of M we find stationary patterns and calculate $\langle u \rangle$. With this process we find some branches and the resulting pattern branches jump from one branch to another. Stationary pattern on one branch to the other differs by the size and heights of the stationary patches. In order to understand the bifurcation behavior, we have performed forward and backward continuations along each branch and we have observed that four of them actually bifurcate from a branch of stationary patterns. The branches of stationary patterns bifurcating from a single branch of stationary solution for the nonlocal model (3.1) against M are presented in Fig. 6. Four branches are plotted with blue, green, red and cyan colour respectively. There exist some other branches also which jump to any one of the branches presented here at small values of M. Such types of branches are not presented here. For the nonlocal model we find stationary pattern at small values of M with $\alpha = 1.9$ and $d = 2$. However the local model is unable to produce any stationary pattern for this parameter set. It clearly indicates that the existence of stationary pattern some time depends upon the initial condition also. Here we find stationary pattern through backward continuation method.

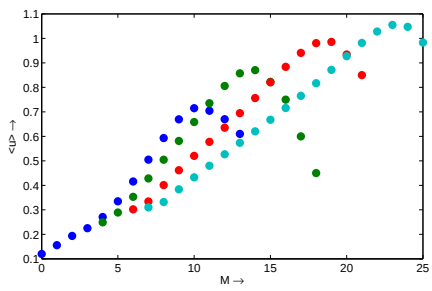

FIGURE 6. Existence of multiple branches of stationary solution with variation in M for the nonlocal model (3.1).

Now we are interested to know what happens if we start with the oscillatory pattern or spatio-temporal chaotic pattern as initial condition and then start increasing the value of M. In other words, we can consider the oscillatory and chaotic patterns as initial condition for the simulation of the nonlocal model (3.1) and perform simulations with $M = 1, 2, 3, \cdots$. Here simulations are performed with the same values of β, γ, δ as mentioned above but $d = 2$. With reference to Fig. 3, we find oscillatory pattern and spatio-temporal chaotic pattern for $\alpha = 2.18$ and $\alpha = 2.23$ respectively for the local model (2.4). If we start from oscillatory pattern and simulate the nonlocal model (3.1) with increasing magnitude of M. In this case we observe the transition from oscillatory pattern to stationary pattern through spatio-temporal chaotic pattern. If we perform the forward and backward continuation method, again we find multiple branches

of stationary solutions bifurcating from the spatio-temporal chaotic pattern. A schematic bifurcation diagram is presented at Fig. 7a. On the other hand, if we start from the chaotic branch, that is with $\alpha = 2.23$, we observe direct transition to stationary patterns. This transition is presented in Fig. 7b. It is quite difficult to construct a complete bifurcation diagram showing transitions from one branch to the other and hence we prevent ourselves from the construction of any more bifurcation diagram. These numerical simulations indicate the existence of stationary patches with the increase in the range of nonlocal interaction.

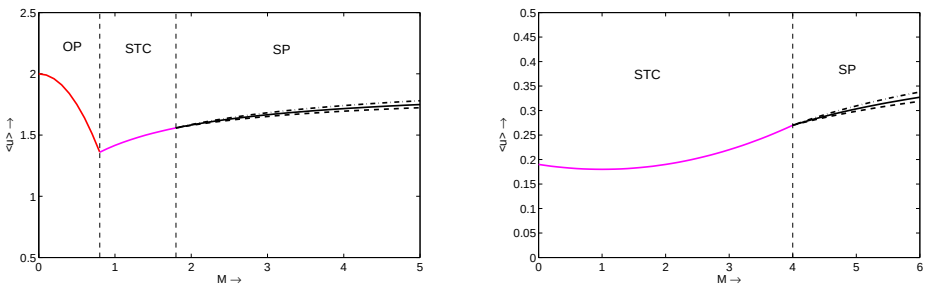

(a) (b)

FIGURE 7. Bifurcation diagrams showing the transition of oscillatory patterns and chaotic patterns to stationary patch patterns with the increase in the magnitude of M. (a) transition from oscillatory to stationary pattern through statio-temporal chaos; (b) transition from spatio-temporal chaotic pattern to stationary pattern. Branches corresponding to oscillatory pattern, spatio-temporal chaotic pattern and stationary pattern are marked with red, magenta and black colour respectively.

Finally we are interested to check whether the increase in the range of nonlocal interaction enhance the parametric domain within which we find stationary pattern. For this purpose we present two pattern diagrams (similar to Fig. 4) to understand the role of nonlocal interaction directly on the spatio-temporal pattern. We simulate the nonlocal model (3.1) with fixed parameter values $\beta = 1$, $\gamma = 0.6$, $\delta = 0.1$, two different values of M and a range of parameter values of α and d. We have chosen $M = 2$ and $M = 5$ respectively and relevant pattern diagrams are presented in Fig. 8. Increase in the range of nonlocal interaction can stabilize the dynamics and also enhance the stationary coexistence. Significant amount of nonlocal interaction can change the oscillatory and chaotic patterns to stationary patches. Further increase in M will results in the stationary pattern for all values of $\alpha \in [1.8, 2.3]$ and $d \in [2, 12]$.

5. Discussion

In this present work we have considered an interacting prey-predator model, with ratio-dependent functional response and density dependent death rate of predators, with nonlocal intra-species interaction among the prey species only. For simplicity we have considered the nonlocal interaction to model the nonlocal consumption of resources by the prey species only. It means that prey individuals can move from one location to another for the consumption of resources and hence compete with the prey individuals present at those location as well coming from nearby locations also. Recently we have worked on a similar model with nonlocal interaction terms in both the population and have reported the stabilizing role of nonlocal interaction and existence of multiple stationary branches only [5]. In another work we have demonstrated the generation of Turing patterns for Rosenzweig-Macarthur model in the presence of nonlocal interaction [7]. Here we have reported a systematic approach to understand the effect of nonlocal interaction on the resulting spatio-temporal pattern. Forward and backward continuation reveals the

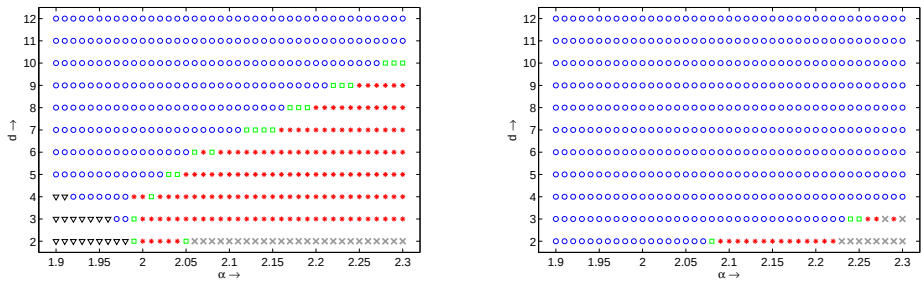

(a) (b)

FIGURE 8. Pattern diagram for $\beta = 1$, $\gamma = 0.6$, $\delta = 0.1$, $M = 2$ and a range of values of α and d. For interpretation of the symbols, see the caption of Fig. 4.

transition of dynamic patterns (oscillatory and chaotic patterns) to stationary patches with the increase in the range of nonlocal interactions.

Recently researchers have worked on couple of spatio-temporal models of interacting populations with nonlocal interaction terms and investigated the existence of traveling wave, periodic traveling wave and modulated traveling waves [1,6,9,20,21]. The influence of the choice of kernel functions on the width and height of the stationary patches is also investigated in some recent literature [14,15]. However, the choice of suitable kernels and estimate for the range of nonlocal interaction depend upon the particular species under consideration [17]. In [22], Tanzy *et al.* have considered the effect of asymmetric kernel function on the resulting patterns due to the nonlocal interaction. The study on the effect of nonlocal interaction on the oscillatory and chaotic pattern as well as the existence of multiple stationary branches is rare [6]. The transition from one type of pattern to another, due to the presence of nonlocal interaction term and increase in the range of nonlocal interactions, is an important topic of research.

Here we have established the existence of stationary patterns when the range of nonlocal interaction is significantly large. Nonlocal interaction also generates stationary patterns for a range of parameter values for which the local model produces homogeneous solution. For example, we found homogeneous steady-state solution produced by the model (2.4), with local interaction, for $\alpha \in [1.9, 1.99]$ and $d = 2$ (see Fig. 3). However we find stationary patterns, which are solutions periodic in space and stationary in time, for the same set of parameter values and $M = 5$ for the nonlocal model (3.1) (see Fig. 8). Existence of stationary patterns for a wide range of parameter values indicates the formation of isolated patches of the population over their habitats, and the number of such patches is determined by the size of the spatial domain as well as the range of nonlocal interaction which is equal to $2M$. Through numerical simulations and continuation technique we have reported the transition from homogeneous steady-state, oscillatory pattern and spatio-temporal chaotic patterns to the stationary patchy patterns for long range of nonlocal interaction. It is important to mention here that one can find stationary patchy patterns for most of the parameter values as presented in Fig. 8(b) however the size of the patches is not the same everywhere.

Here we have reported the existence of multiple branches of stationary solutions depending upon the magnitude of M. Increase in the range of nonlocal interaction results in the overlap of nearby foraging areas and hence alters the size of the localized patches. This phenomena is responsible for the existence of multiple stationary patterns obtained through numerical continuations [5, 6]. With the advancement of time individuals of the prey species can attempt to extend their range of nonlocal movement to have access to the resources lying just outside of the established patches and this ecological phenomenon results in the transition from one branch of stationary solution to the other branch. This phenomenon resulting

from the nonlocal modelling approach can be accepted as the explanation of evolutionary change in the sizes of existing population patches.

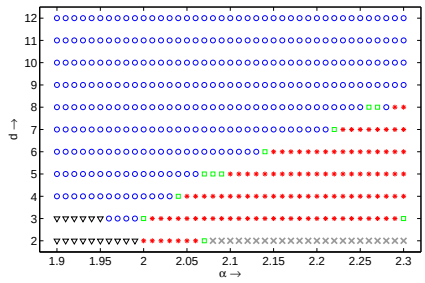

FIGURE 9. Pattern diagram for the nonlocal model (3.1) but with Gaussian kernel. Parameter values are $\beta = 1$, $\gamma = 0.6$, $\delta = 0.1$, $\sigma = 2$. Interpretation of the symbols are same as in Fig. 4.

The analytical results and supportive numerical simulations are based upon the particular choice of the kernel function ϕ. One can raise the question whether the transition of patterns from one type to another is true for other choices of the kernel function or not. For the chosen kernel function ϕ, the strength of nonlocal interaction is the same with the range $[x-M,\ x+M]$. In reality the strength of interaction may depend on the distance of the resource from the current position of the individual. In order to take care of this aspect, researchers have considered different types of kernel functions [14,15,20]. Similar question can be raised for the existence of stationary patterns for most of the parameter values for other choice of the kernel functions. To answer this question we have prepared a pattern diagram (like Fig. 8) for the kernel function $\phi_2(z) = e^{-\frac{|z|}{\sigma}}/2\sigma$. This kernel function is known as Gaussian kernel [14]. The pattern diagram is prepared for the parameter same parameter values we have used earlier, that is, $\beta = 1$, $\gamma = 0.6$, $\delta = 0.1$ and $\sigma = 2$, in the $\alpha - d$-parameter space. Resulting pattern diagram is presented in Fig. 9. Comparison of the pattern diagrams in Fig. 8b and Fig. 9 reveals that the two different choices of kernel functions can produce similar pattern diagrams. We find stationary patterns for all values of $\alpha \in [1.9, 2.3]$ and $d \in [2, 12]$ when M and σ are greater than 8. We have observed similar type of transitions from dynamic oscillatory and chaotic patterns to multiple branches of stationary solutions for Gaussian kernel also. However the transition point may differ slightly when compared with two different kernels. In summary, the main finding of this work that the nonlocal interaction can enhance the existence stationary solutions for a wide range of parameter values.

Acknowledgements. Lai Zhang gratefully acknowledges the financial support from the PRC Grant NSFC 11571301. Numerical simulations were performed on resources provided by the Swedish National Infrastructure for Computing (SNIC) at High Performance Computing Center North (HPC2N).

References

[1] N. Apreutesei, N. Bessonov, V. Volpert, V. Vougalter. *Spatial structures and generalized travelling waves for an integro-differential equation.* DCDS B, 13(3) (2010), 537–557.

[2] M. Banerjee, S. Abbas. *Existence and non-existence of spatial patterns in a ratio-dependent predator-prey model.* Ecol. Comp., 21 (2015), 199–214.

[3] M. Banerjee, S. Banerjee. *Turing instabilities and spatio-temporal chaos in ratio-dependent Holling-Tanner model.* Math. Biosci., 236 (2012), 64–76.

[4] M. Banerjee, S. Petrovskii. *Self-organized spatial patterns and chaos in a ratio-dependent predator-prey system.* Theor. Ecol., 4 (2011) 37–53.

[5] M. Banerjee, M. Sen, V. Volpert. Pattern formation in a prey-predator model with nonlocal interaction terms. In "Applied Analysis with Application in Biological and Physical Sciences", Springer, In press, 2016.

[6] M. Banerjee, V. Volpert. *Prey-predator model with a nonlocal consumption of prey.* Chaos, 26 (2016), 083120.

[7] M. Banerjee, V. Volpert. *Spatio-temporal pattern formation in Rosenzweig-Macarthur model: effect of nonlocal interactions.* (under review) (2016).

[8] N. Bessonov, N. Reinberg, V. Volpert. *Mathematics of Darwin's diagram.* Math. Model. Nat. Phenom., 9(3) (2014), 5–25.

[9] N. F. Britton. *Spatial structures and periodic travelling waves in an integro-differential reaction-diffusion population model.* SIAM J. Appl. Math., 6 (1990) 1663–1688.

[10] S. Genieys, V. Volpert, P. Auger. *Pattern and waves for a model in population dynamics with nonlocal consumption of resources.* Math. Model. Nat. Phenom., 1(1) (2006) 63–80.

[11] Y. A. Kuznetsov. Elements of Applied Bifurcation Theory. Springer-Verlag, New York 2004.

[12] H. Malchow. *Spatio-temporal pattern formation in nonlinear nonequilibrium plankton dynamics.* Proc. Royal Soc. London B, 251 (1993), 103–109.

[13] A. Medvinsky, S. Petrovskii, I. Tikhonova, H. Malchow, B. L. Li. *Spatiotemporal complexity of plankton and fish dynamics.* SIAM Rev, 44 (2002), 311–370.

[14] S. M. Merchant, W. Nagata. *Instabilities and spatiotemporal patterns behind predator invasions with nonlocal prey competition.* Theor. Pop. Biol., 80 (2011), 289–297.

[15] S. M. Merchant, W. Nagata. *Selection and stability of wave trains behind predator invasions in a model with non-local prey competition.* IMA J. Appl. Math., 80 (2015), 1155–1177.

[16] J. D. Murray. Mathematical Biology II. Springer-Verlag, Heidelberg (2002).

[17] R. Nathan, E. Klein, J. J. Robledo-Arnuncio. *Dispersal kernels: Review, in Dispersal Ecology and Evolution.* J. Clobert, M. Baguette, T. G. Benton, and J. M. Bullock, (Eds.), Oxford University Press, Oxford, UK, (2012) 187–210.

[18] A. Okubo, S. Levin. Diffusion and Ecological Problems: Modern Perspectives. Springer, Berlin 2001.

[19] Perko, L. Differential Equations and Dynamical Systems. Springer, New York, 2001.

[20] B. L. Segal, V. A. Volpert, A. Bayliss. *Pattern formation in a model of competing populations with nonlocal interactions.* Phys. D, 253 (2013) 12–23.

[21] J. A. Sherratt. *Periodic traveling waves in integro-differential equations for nonlocal dispersal.* SIAM J. Appl. Dyna. Sys., 13(4) (2014) 1517–1541.

[22] M. C. Tanzy, V. A. Volpert, A. Bayliss, M. E. Nehrkorn. *Stability and pattern formation for competing populations with asymmetric nonlocal coupling.* Math. Biosci., 246 (2013), 14–26.

[23] V. Volpert. Elliptic Partial Differential Equations, Volume 2, Reaction-diffusion Equations. Birkhauser, 2014.